High-precision $B(E2)$ measurements of semi-magic ^{58,60,62,64}Ni by Coulomb excitation

J. M. Allmond,[1] B. A. Brown,[2,3] A. E. Stuchbery,[4] A. Galindo-Uribarri,[5,6] E. Padilla-Rodal,[7] D. C. Radford,[5] J. C. Batchelder,[8] M. E. Howard,[9] J. F. Liang,[5] B. Manning,[9] R. L. Varner,[5] and C.-H. Yu[5]

[1]*JINPA, Oak Ridge National Laboratory, Oak Ridge, Tennessee 37831, USA*
[2]*National Superconducting Cyclotron Laboratory, Michigan State University, East Lansing, Michigan 48824, USA*
[3]*Department of Physics and Astronomy, Michigan State University, East Lansing, Michigan 48824, USA*
[4]*Department of Nuclear Physics, Australian National University, Canberra ACT 0200, Australia*
[5]*Physics Division, Oak Ridge National Laboratory, Oak Ridge, Tennessee 37831, USA*
[6]*Department of Physics and Astronomy, University of Tennessee, Knoxville, Tennessee 37996, USA*
[7]*Instituto de Ciencias Nucleares, UNAM, AP 70-543, 04510 Mexico, D.F., Mexico*
[8]*UNIRIB, Oak Ridge Associated Universities, Oak Ridge, Tennessee 37831, USA*
[9]*Department of Physics and Astronomy, Rutgers University, New Brunswick, New Jersey 08903, USA*

(Received 13 May 2014; revised manuscript received 7 August 2014; published 15 September 2014)

High-precision reduced electric-quadrupole transition probabilities $B(E2;0_1^+ \rightarrow 2_1^+)$ have been measured from single-step Coulomb excitation of semi-magic ^{58,60,62,64}Ni ($Z = 28$) beams at 1.8 MeV per nucleon on a natural carbon target. The energy loss of the nickel beams through the carbon target were directly measured with a zero-degree Bragg detector and the absolute $B(E2)$ values were normalized by Rutherford scattering. The $B(E2)$ values disagree with recent lifetime studies that employed the Doppler-shift attenuation method. The present high-precision $B(E2)$ values reveal an asymmetry about ^{62}Ni, midshell between $N = 28$ and 40, with larger values towards ^{56}Ni ($Z = N = 28$). The experimental $B(E2)$ values are compared with shell-model calculations in the full pf model space and the results indicate a soft ^{56}Ni core.

DOI: 10.1103/PhysRevC.90.034309 PACS number(s): 25.70.De, 23.20.−g, 21.10.Ky, 27.50.+e

I. INTRODUCTION

The standard shell closures of Z or N equal to 2, 8, 20, 28, 50, 82, or 126 [1,2] and subshell closures such as 40 and 64 are subject to change as one moves to exotic nuclei and extreme N/Z ratios. For example, a breakdown of the $N = 20$ shell closure in ^{31}Na [3] and ^{32}Mg [4], and $N = 28$ shell closure in ^{44}S [5–8] have been observed. On the other hand, the $Z = 50$, $N = 82$ double-shell closure of radioactive ^{132}Sn is robust [9–15]. However, reduced quadrupole transition probabilities $B(E2;0_1^+ \rightarrow 2_1^+)$ for the Sn isotopes have shown enhanced 2_1^+ collectivity when moving from midshell, which neighbors a potential $N = 64$ subshell, to radioactive $Z = N = 50$ (cf. Bader *et al.* [16] and references within). The evolution of nuclear shell structure has been of immense interest since the advent of fast and reaccelerated radioactive ion beams. The Ni and Sn isotopes, which both span across two radioactive double-shell closures with potential subshell closures in-between, have been of particular interest in the past decade. The Ni isotopes span the radioactive double-shell closures of ^{56}Ni ($Z = N = 28$) and ^{78}Ni ($Z = 28$, $N = 50$) with a potential subshell closure at $N = 40$, ^{68}Ni (cf. shell-model diagram in Fig. 1).

Radioactive ^{56}Ni and ^{68}Ni have comparatively large 2_1^+ energies and small $B(E2)$ values [17,18], which alone suggest good $N = 28$ and $N = 40$ shell and subshell closures, respectively. However, discontinuities in neutron separation energies show weak to no evidence for a $N = 40$ subshell closure for ^{68}Ni [19,20]. Furthermore, a $B(E2)$ maximum would be expected at midshell, ^{62}Ni. The situation near midshell is complicated by $B(E2)$ discrepancies between recent Doppler-shift attenuation method (DSAM) experiments on the stable Ni isotopes [21–23] and the 2001 comprehensive data evaluation of Raman *et al.* [24]. In particular, $B(E2;0_1^+ \rightarrow 2_1^+)$ values of ^{58,60,62,64}Ni were reported by Kenn *et al.* [21] with a precision that ranges from 1.4 to 3.5 % and values that are several standard deviations from the 2001 evaluation [24]. Other recent DSAM studies [22,23], which are not high precision, appear more consistent with the study by Kenn *et al.* [21].

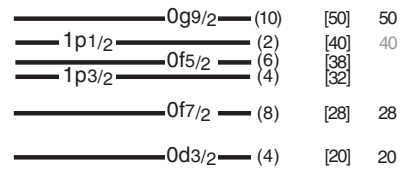

FIG. 1. Single-particle states with shell closures at 20, 28, and 50, and a subshell closure at 40.

Discrepancies in the stable Ni $B(E2)$ values are not only a problem for understanding the structure of the Ni isotopes near midshell, but also in having a dependable reference point in which to discuss trends of the radioactive Ni isotopes. Furthermore, $B(E2)$ values of radioactive ^{106,108,110}Sn were measured relative to ^{58}Ni [25,26], which would show much less enhancement if normalized to the value by Kenn *et al.* [21]. In this paper, high-precision absolute $B(E2;0_1^+ \rightarrow 2_1^+)$ values are reported from single-step Coulomb excitation of semi-magic ^{58,60,62,64}Ni in inverse kinematics, which disagree with the recent DSAM studies [21–23]. Similar discrepancies exist for the stable Sn isotopes [24,27], which will be discussed in a future publication [28].

II. EXPERIMENT

A method for measuring the Coulomb excitation of stable or radioactive ion beams using inverse kinematics

($A_{\text{projectile}} > A_{\text{target}}$) has been developed at the Holifield Radioactive Ion Beam Facility (HRIBF) [11,29]. With this method, scattered target nuclei are measured at forward laboratory angles relative to the beam direction (corresponding to backward angles in the center-of-mass frame) to provide a clean trigger for selecting the γ-ray transitions from the Coulomb-excited beam and to normalize the integrated beam current through Rutherford scattering. While this technique was primarily developed for radioactive ion beams, there are distinct advantages in employing this technique with stable beams including: (1) it can deliver isotopically pure beams and use relatively pure targets (e.g., $^{\text{nat}}$C is 98.9% ^{12}C), and (2) the recoiling target nuclei are measured at backward center of mass angles where the Rutherford cross section is less sensitive to angle. Back angles minimize uncertainties related to geometry, and also maximize the ratio of Coulomb excitation to Rutherford scattering, which minimizes the nonprompt (or random) particle-γ component.

Semi-magic ^{58,60,62,64}Ni beams at an energy of 1.8 MeV per nucleon were Coulomb excited on a $\sim$1 mg/cm^2 natural carbon target over a period of 4 d. The beams were provided by the 25-MV tandem accelerator at the HRIBF. The energy loss of the ^{58}Ni and ^{60}Ni beams through the carbon target at 1.8 MeV per nucleon were measured by a Bragg detector at zero degrees and resulted in 42.7(8) MeV and 42.1(8) MeV energy loss, respectively. The Bragg detector was calibrated by measuring direct beam from the tandem at multiple energies, which was achieved quickly by dropping charge states while keeping the magnetic rigidity fixed.

Recoiling target nuclei were detected in the BareBall array [30] using two rings of CsI crystals with minimal absorbers. Ring 2 has 10 CsI crystals at angles of 14°–28° relative to the beam direction and ring 3 has 12 CsI crystals at angles of 28°–44°. Coincident γ rays were detected by the CLARION array [31] using nine segmented HPGe clover detectors at angles of 90° (five clovers), 132° (three clovers), and 154° (one clover). The clover detectors were at a distance of 21.75 cm from the target with a total efficiency of 2.44(6)% at 1 MeV, 2.24(5)% at 1.173 MeV, and 2.08(5)% at 1.333 MeV. The experimental trigger required either a scaled-down particle event or a particle-γ coincidence event. The trigger type was recorded for each event in a bit register to cleanly distinguish particles from the scaled-down trigger and particle-γ trigger. A relatively low beam intensity of $\sim$5 pA was used to prevent target damage and to maintain a data acquisition live time of $\geqslant$ 99%. The particle-gated $2_1^+ \rightarrow 0_1^+$ γ-ray transitions of ^{58,60,62,64}Ni from Coulomb excitation are shown in Fig. 2. The relatively high efficiency of the particle-γ coincidence trigger and high resolution of CLARION provide an excellent tag of the 2_1^+ states.

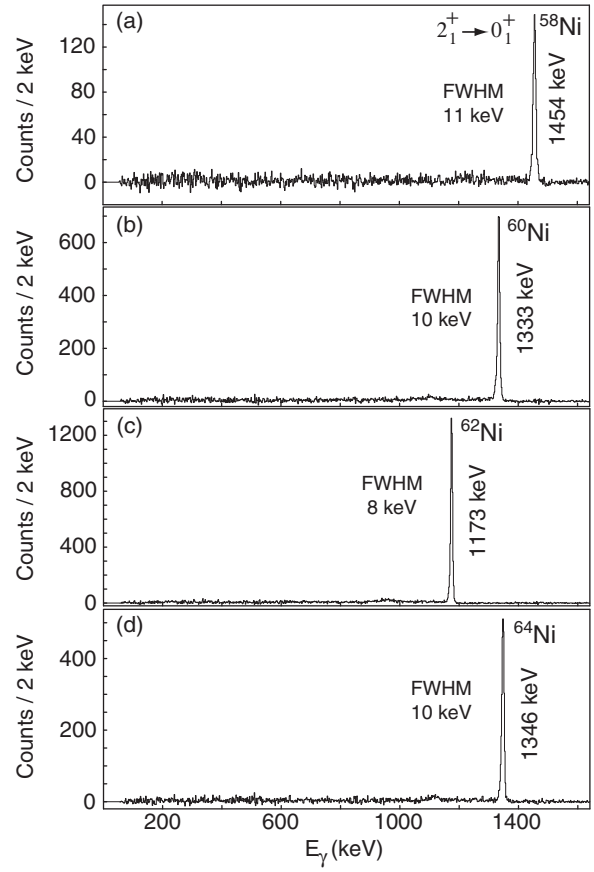

FIG. 2. The carbon gated and Doppler corrected $2_1^+ \rightarrow 0_1^+$ γ-ray transitions of ^{58,60,62,64}Ni from Coulomb excitation and decay.

III. ANALYSIS AND RESULTS

The reduced $E2$ matrix elements for ^{58,60,62,64}Ni can be obtained approximately from the data using the following relation in second-order perturbation theory [32]:

$$\frac{\sigma_{\text{Coulex}}(2_1^+)}{\sigma_{\text{Ruth}}} \approx N\langle 0_1||M(E2)||2_1\rangle^2[1 + K\langle 2_1||M(E2)||2_1\rangle], \quad (1)$$

where $\sigma_{\text{Coulex}}(2_1^+)$ is the 2_1^+ Coulomb-excitation cross section, σ_{Ruth} is the Rutherford cross section, and N and K are scale factors dependent on the kinematics of the projectile/target combination. The reduced transition probability and static quadrupole moment are related to the reduced $E2$ matrix elements by

$$B(E2; 0_1^+ \rightarrow 2_1^+) = \langle 0_1||M(E2)||2_1\rangle^2 \quad (2)$$

and

$$Q(2_1^+) = 0.7579\,\langle 2_1||M(E2)||2_1\rangle. \quad (3)$$

At least two different targets, beam energies, or center-of-mass angles are generally required to solve for both $\langle 0_1||M(E2)||2_1\rangle$ and $\langle 2_1||M(E2)||2_1\rangle$ in Eq. (1). However, the 2_1^+ quadrupole moments are expected to be zero [33,34]. Furthermore, the scale factor K in Eq. (1) is relatively small for the low-Z carbon target data, $K \sim 0.17$. For instance, a quadrupole moment of 0.1 eb, a reasonable upper limit on the magnitude [33–35], would only have a $\sim$2% effect on the extracted $B(E2)$. In the present study, the cross sections are calculated with the Coulomb excitation (Coulex) code GOSIA [36]. The GOSIA calculations are not limited to second-order perturbation theory, cf. Eq. (1). Furthermore, the GOSIA calculations include the following corrections to the Coulex cross sections and γ-ray angular distributions (cf. Fig. 3) [36]: dipole polarization correction, kinematic correction to the solid angle, nuclear

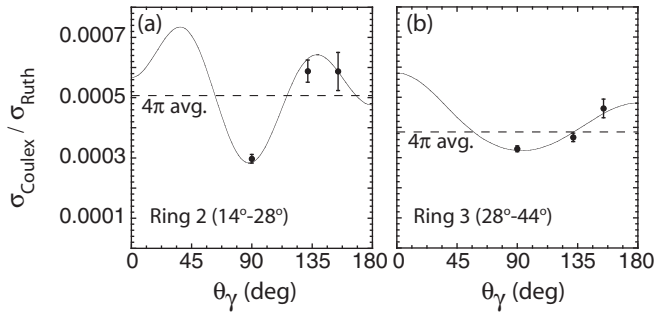

FIG. 3. The $2_1^+ \rightarrow 0_1^+$ γ-ray angular distributions for ^{64}Ni, gated on the carbon target recoils in (a) BareBall ring 2 and (b) BareBall ring 3.

deorientation correction, and finite-size γ detector correction. The deorientation correction was essentially negligible. The $\Delta\phi$ particle-γ angular correlations were analyzed using the recoil-in-vacuum (RIV) technique (see Refs. [12,14]) but the low recoil velocity, low average charge state, and small 2_1^+ lifetime and g factor [34] resulted in no observed attenuation.

The extracted $\langle 0_1||M(E2)||2_1\rangle$ matrix elements for ^{58,60,62,64}Ni are given per BareBall ring in Table I with only the statistical uncertainties. The two rings show excellent consistency in the extracted $E2$ matrix elements with no systematic difference. A nonzero quadrupole moment or nuclear interference would have resulted in a systematic difference between the extracted matrix elements from each ring, which is not observed. A summary of the final $E2$ matrix elements and $B(E2)$ values for ^{58,60,62,64}Ni is also given in Table I. The total error includes systematic uncertainties from the efficiency, energy loss of the beam, detector geometry, and static quadrupole moment. Each systematic error was roughly 1% for the $E2$ matrix elements and 2% for $B(E2)$ values. The Bragg detector measurements of the beam energy-loss through the target were particularly critical in achieving high precision and controlling systematic errors from target thicknesses and stopping powers.

Figure 4 shows the present $B(E2)$ values compared with the 2001 evaluation of Raman *et al.* [24] and the DSAM studies by Kenn *et al.* [21], Orce *et al.* [22], and Chakraborty *et al.* [23]. The recent DSAM studies indicate a $B(E2)$ maximum at ^{62}Ni, midshell between $N = 28$ and 40, which disagree with the 2001 evaluation of Raman *et al.* [24] and the present results. These DSAM studies were not included in the 2001 evaluation of Raman *et al.* [24] but have been included in a

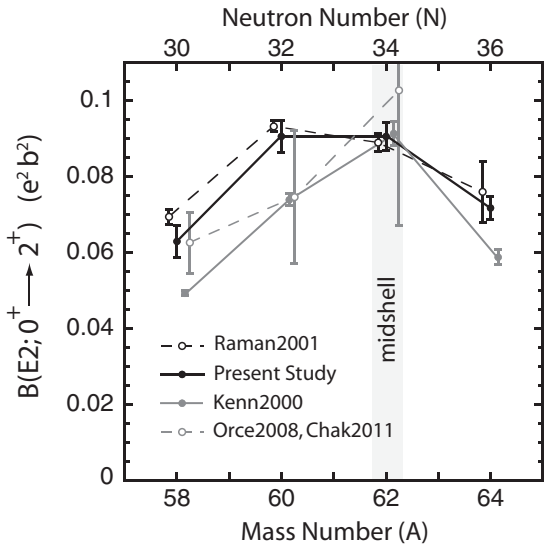

FIG. 4. $B(E2; 0_1^+ \rightarrow 2_1^+)$ systematics of the stable Ni isotopes from the present study compared to Raman2001 [24] and the recent DSAM studies Kenn2000 [21], Orce2008 [22], and Chak2011 [23].

2012 evaluation of the $N \sim Z \sim 28$ region [37]. The $B(E2)$ values of the present study, which are consistent with the Raman evaluation [24] but provide a much more precise $B(E2)$ for ^{64}Ni, indicate a smoother profile with an asymmetry about ^{62}Ni, where ^{60}Ni and ^{62}Ni have essentially the same electric quadrupole transition strength; ^{64}Ni has a significantly lower $B(E2)$ than ^{60}Ni. The simple expectation is that if $N = 28$ and $N = 40$ are robust shell and subshell closures, then the maximum $B(E2)$ should be at midshell where the valence space is ideally maximized. The $B(E2)$ values of ^{58,60}Ni, approaching $Z = N = 28$, are enhanced with respect to ^{62}Ni (midshell) and ^{64}Ni, similar to the data on the Sn $B(E2)$ values approaching $Z = N = 50$ (cf. Bader *et al.* [16] and references within).

IV. DISCUSSION

Experimental and theoretical $B(E2)$ values for the $N = 28$ isotones and Ni ($Z = 28$) isotopes are compared in Fig. 5. The experimental data are from the present study and the recent $N \sim Z \sim 28$ evaluation [37], which includes the recent Coulomb excitation studies of radioactive ^{66,68}Ni by Sorlin *et al.* [18], ^{54,56}Ni by Yurkewicz *et al.* [17], ^{70}Ni by Perru *et al.* [38], and ^{68}Ni by Bree *et al.* [39]; only model-independent

TABLE I. Summary of $E2$ matrix elements and $B(E2)$s.

$Z = 28$	N	$\langle 0_1^+\|\|M(E2)\|\|2_1^+\rangle$ eb^a		$\langle 0_1^+\|\|M(E2)\|\|2_1^+\rangle$ eb^b	$B(E2; 0_1^+ \rightarrow 2_1^+) e^2b^{2b}$
		Ring 2	Ring 3		
^{58}Ni	30	(+) 0.2532(79)	(+) 0.2506(49)	(+) 0.251(8)	0.0630(40)
^{60}Ni	32	(+) 0.3008(47)	(+) 0.3018(30)	(+) 0.301(7)	0.0906(41)
^{62}Ni	34	(+) 0.3038(37)	(+) 0.3002(24)	(+) 0.301(6)	0.0906(37)
^{64}Ni	36	(+) 0.2626(47)	(+) 0.2708(30)	(+) 0.268(5)	0.0718(29)

[a]Statistical uncertainties.
[b]Statistical and systematic uncertainties.

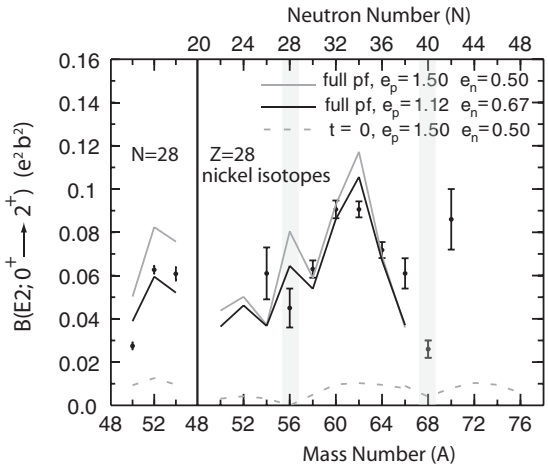

FIG. 5. Comparison of experimental and theoretical $B(E2;0_1^+ \rightarrow 2_1^+)$ values for the $N = 28$ isotones and the nickel isotopes (see text). The experimental data are from the present study and Pritychenko2012 evaluation [37].

results are given here. The theoretical results were obtained with the GXPF1A Hamiltonian [40,41] for protons and neutrons in the full pf model space ($0f_{7/2}$, $0f_{5/2}$, $1p_{3/2}$, $1p_{1/2}$) using two different sets of effective charges. Wave functions with J-scheme dimensions up to 10^8 were obtained with the code NUSHELLX [42]. The GXPF1 Hamiltonian [40] was obtained starting with a set of two-body matrix elements derived from the Bonn-C potential [43]. Seventy linear combinations of the four single-particle energies and 195 two-body matrix elements were then fitted to 699 binding energies and excitation energies for nuclei in the pf shell. For the GXPF1A Hamiltonian [41], five of the $T = 1$ GXPF1 two-body matrix elements were modified to improve the energies for the neutron-rich isotopes of Ca, Ti, and Fe. For comparison, the pf shell results obtained when no excitations are allowed across the $N = 28$ gap are also shown, i.e., the "$t = 0$" truncation. For $A \geqslant 66$ the $t = 0$ results were also obtained in the $0f_{5/2}$, $1p_{3/2}$, $1p_{1/2}$, $0g_{9/2}$ model space for neutrons with the Hamiltonian obtained in Ref. [44]. This Hamiltonian was obtained starting with a set of two-body matrix elements derived from the Bonn-C potential [43]. Twenty linear combinations of the four single-particle energies and the 65 two-body matrix elements were then fitted to 104 binding energies and excitation energies for $^{57-78}$Ni [44]. In the NUSHELLX interaction library [42], this model space is called jj44pn and the Hamiltonian is called jj44pna.

Harmonic oscillator radial wave functions with $\hbar\omega = 45A^{-1/3}–25A^{-2/3}$ are adequate to use at the level of about 10% accuracy. For the effective charges $e_p = 1 + \delta e_p$ and $e_n = \delta e_n$, the "standard" isoscalar core-polarization effective charges of $\delta e_p = \delta_n = 0.5$ were used first (cf. original calculations with GXPF1A [40,41]). These were combined with the model space $E2$ amplitudes A_p and A_n to give the total $B(E2; I_i \rightarrow I_f) = [A_p e_p + A_n e_n]^2/(2J_i + 1)$ [45]. The effective charges arise from the perturbative coupling of the nucleons in the model space with $\Delta N = 2$ particle-hole excitations, where $N = 2n + \ell$ in the harmonic oscillator.

The $t = 0$ calculations are far below the data (cf. dashed lines in Fig. 5). With the $t = 0$ truncation, many of the $\Delta N = 0$ configurations that are important for the $B(E2)$ are left out. In the early analysis of $B(E2)$ data below $A = 56$ in the $f_{7/2}$ model space [46], a large proton effective charge of about $e_p \approx 2.2$ for $N = 28$ was needed to compensate for the $t = 0$ truncation. A neutron effective charge of $e_n = 1.0$ was used for the heavy nickel [44] and tin isotopes [47]. However, near ^{56}Ni (and ^{100}Sn [16]), the experimental $B(E2)$ values are even larger than those obtained with $t = 0$ and $e_n = 1.0$. For the nickel isotopes this enhancement is explained by the expansion to the full pf model space. Within the full pf model space, the enhancement can be traced to two mechanisms: (A) mixing with one-particle one-hole excitations across the $N = 28$ gap that can approximately be treated as a core-polarization contribution to the effective charges for the entire chain of nickel isotopes, and (B) mixing with low-lying deformed bands around ^{56}Ni that arise from many-particle many-hole excitations across the $N = 28$ gap. For example, there is a "4p-4h" band in ^{56}Ni starting around 4.5 MeV [48]. It is low in energy due to the two-proton two-neutron α-type correlation in this configuration. For this deformed band in ^{56}Ni, $B(E2;0_1^+ \rightarrow 2_1^+) = 0.21\ e^2\text{b}^2$ (off the scale of Fig. 5). The calculated $B(E2)$ for low-lying states near ^{56}Ni are enhanced due to the partial mixing of spherical and deformed configurations.

The calculated results depend on the effective charges. The $B(E2)$ data for the mirror $27/2^-$ to $23/2^-$ transitions in ^{51}Fe and ^{51}Mn can be used to determine the t_z dependence of the effective charges [49]. In order to reproduce the experimental $B(E2)$ values of 0.00413(24) $e^2\text{b}^2$ and 0.00467(14) $e^2\text{b}^2$ [49], respectively, in the full pf model space, $\delta e_p = 0.12$ and $\delta e_n = 0.67$ are required. The results obtained with these effective charges are given by the solid black lines in Fig. 5. The agreement with experiment improves for most cases.

The $B(E2)$ data for mirror transitions in $A = 43$–45 are in best agreement with effective charges of $e_p = 1.20$ and $e_n = 0.55$ [50]. One of the earliest analyses of $E2$ transitions in the lower part of the pf shell gave $e_p = 1.16(16)$ and $e_n = 0.45(3)$ [46]. It is expected that $\delta e_n > \delta e_p$ due to the repulsive contribution of the giant isovector quadrupole resonance [45]. Microscopically derived $\Delta N = 2$ effective charges are nucleus and orbital dependent [51]. For the dominant contributions involving the $f_{7/2}$-$f_{7/2}$ and $f_{7/2}$-$p_{3/2}$ orbital combinations in the titanium isotopes, Ma *et al.* [51] obtained $e_p \approx 1.30$ and $e_n \approx 0.5$–0.6.

There is a relatively large disagreement between experiment and theory for ^{54}Ni and ^{56}Ni, but the experimental uncertainties are large and the data should be confirmed. For $A \geqslant 66$ the calculations in the jj44 model space require at least a neutron effective charge of $e_n = 1.0$ (as needed for the 8^+ to 6^+ transition in ^{70}Ni [44]) whose increase over $e_n = 0.6$ could be interpreted in terms of a core-polarization contribution of one-particle one-hole protons across $N = 28$ (mechanism A above). The theoretical $B(E2;0_1^+ \rightarrow 2_1^+)$ for ^{70}Ni obtained with $e_n = 1.0$ is a factor of 2–3 smaller than experiment. Tsunoda *et al.* [52] have expanded the jj44 model space by adding $1d_{5/2}$ orbital for neutrons and allowing excitations from $0f_{7/2}$ for both protons and neutrons. Their $B(E2)$ results

shown in Fig. 1 of Ref. [52] are consistent with our results up to $N = 38$ (^{66}Ni). Their results for ^{68,70}Ni are a factor of 2–3 smaller than experiment. The experimental $B(E2)$ for ^{70}Ni should be confirmed.

Coraggio *et al.* [53] have also added $1d_{5/2}$ orbital for neutrons and allow excitations from $0f_{7/2}$ only for protons to the $1p_{3/2}$ orbital. Their results for $N \geqslant 34$ are similar to those of Tsunoda *et al.* [52]. Their calculation does not conserve isospin and this particularly affects ^{56}Ni where both proton and neutron excitations from $0f_{7/2}$ should be included. For $N = 30$–32 their $B(E2)$ values are smaller than experiment.

In conclusion, high-precision absolute $B(E2; 0_1^+ \rightarrow 2_1^+)$ values were measured from single-step Coulomb excitation of semi-magic ^{58,60,62,64}Ni, which disagree with recent DSAM studies [21–23]. The present $B(E2)$ results are consistent with the 2001 evaluation of Raman *et al.* [24], which preserves the $B(E2)$ enhancement of radioactive ^{106,108,110}Sn [25,26], measured relative to ^{58}Ni. However, the present results provide a much more precise $B(E2)$ for ^{64}Ni. The high-precision Ni $B(E2)$ values reveal an asymmetry about ^{62}Ni, midshell between $N = 28$ and 40, with larger values towards ^{56}Ni ($Z = N = 28$). Large-basis shell-model calculations indicate that the full pf shell is required to explain the overall magnitude of the Ni $B(E2)$ values, with the excitation of several nucleons out of the ^{56}Ni ($Z = N = 28$) core. The calculations reproduce the observed $B(E2)$ asymmetry about midshell but maintain a pronounced maximum at midshell, which disagrees with experiment.

ACKNOWLEDGMENTS

The authors gratefully acknowledge D. Cline, A. B. Hayes, R. Grzywacz, N. Warr, and J. L. Wood for fruitful discussions, and J. P. Greene (Argonne National Laboratory) for making the carbon target. The HRIBF operations staff deserve special acknowledgment for providing two beams simultaneously for this experiment as well as a radioactive decay experiment on ^{86}Ga [54]. This research was sponsored by the Office of Nuclear Physics, U.S. Department of Energy, by the Australian Research Council under Grant No. DP0773273, by the U.S. National Science Foundation under Grant No. PHY-1068217, and by CONACyT (Mexico) under Grant No. CB103366. This work was also supported in part by the U.S. DOE under Contracts No. DE-AC05-76OR00033 (UNIRIB), DE-FG02-96ER40983 (UTK), and DE-FG52-08NA28552 (Rutgers). Computational work in support of this research was performed at Michigan State University's High Performance Computing Facility.

[1] M. G. Mayer, Phys. Rev. **74**, 235 (1948).
[2] M. G. Mayer and J. H. D. Jensen, *Theory of Nuclear Shell Structure* (Wiley, New York, 1955).
[3] C. Thibault *et al.*, Phys. Rev. C **12**, 644 (1975).
[4] D. Guillemaud-Mueller *et al.*, Nucl. Phys. A **426**, 37 (1984).
[5] O. Sorlin *et al.*, Phys. Rev. C **47**, 2941 (1993).
[6] H. Scheit *et al.*, Phys. Rev. Lett. **77**, 3967 (1996).
[7] T. Glasmacher *et al.*, Phys. Lett. B **395**, 163 (1997).
[8] D. Sohler *et al.*, Phys. Rev. C **66**, 054302 (2002).
[9] J. R. Beene *et al.*, Nucl. Phys. A **746**, 471c (2004); D. C. Radford *et al.*, *ibid.* **752**, 264c (2005).
[10] K. L. Jones *et al.*, Nature **465**, 454 (2010).
[11] J. M. Allmond *et al.*, Phys. Rev. C **84**, 061303(R) (2011).
[12] J. M. Allmond *et al.*, Phys. Rev. C **87**, 054325 (2013).
[13] J. Van Schelt *et al.*, Phys. Rev. Lett. **111**, 061102 (2013).
[14] A. E. Stuchbery *et al.*, Phys. Rev. C **88**, 051304(R) (2013).
[15] J. M. Allmond *et al.*, Phys. Rev. Lett. **112**, 172701 (2014).
[16] V. M. Bader *et al.*, Phys. Rev. C **88**, 051301(R) (2013).
[17] K. L. Yurkewicz *et al.*, Phys. Rev. C **70**, 054319 (2004).
[18] O. Sorlin *et al.*, Phys. Rev. Lett. **88**, 092501 (2002).
[19] C. Guénaut *et al.*, Phys. Rev. C **75**, 044303 (2007).
[20] S. Rahaman *et al.*, Eur. Phys. J. A **34**, 5 (2007).
[21] O. Kenn, K.-H. Speidel, R. Ernst, J. Gerber, N. Benczer-Koller, G. Kumbartzki, P. Maier-Komor, and F. Nowacki, Phys. Rev. C **63**, 021302(R) (2000); O. Kenn, K.-H. Speidel, R. Ernst, J. Gerber, P. Maier-Komor, and F. Nowacki, *ibid.* **63**, 064306 (2001).
[22] J. N. Orce, B. Crider, S. Mukhopadhyay, E. Peters, E. Elhami, M. Scheck, B. Singh, M. T. McEllistrem, and S. W. Yates, Phys. Rev. C **77**, 064301 (2008).
[23] A. Chakraborty *et al.*, Phys. Rev. C **83**, 034316 (2011).
[24] S. Raman, C. W. Nestor, and P. Tikkanen, At. Data Nucl. Data Tables **78**, 1 (2001).
[25] J. Cederkäll *et al.*, Phys. Rev. Lett. **98**, 172501 (2007).
[26] A. Ekström *et al.*, Phys. Rev. Lett. **101**, 012502 (2008).
[27] A. Jungclaus *et al.*, Phys. Lett. B **695**, 110 (2011).
[28] J. M. Allmond *et al.* (unpublished).
[29] D. C. Radford *et al.*, Phys. Rev. Lett. **88**, 222501 (2002).
[30] A. Galindo-Uribarri, AIP Conf. Proc. **1271**, 180 (2010).
[31] C. J. Gross *et al.*, Nucl. Instrum. Methods Phys. Res. A **450**, 12 (2000).
[32] K. Alder and A. Winther, *Coulomb Excitation* (Academic Press, New York, 1966), pp. 113–116, 305.
[33] D. Cline, H. S. Gertzman, H. E. Gove, P. M. S. Lesser, and J. J. Schwartz, Nucl. Phys. A **133**, 445 (1969).
[34] Evaluated Nuclear Structure Data File (ENSDF), http://www.nndc.bnl.gov/ensdf/.
[35] J. M. Allmond, Phys. Rev. C **88**, 041307(R) (2013).
[36] T. Czosnyka *et al.*, Bull. Am. Phys. Soc. **28**, 745 (1983); http://www.pas.rochester.edu/~cline/Gosia/.
[37] B. Pritychenko, J. Choquette, M. Horoi, B. Karamy, and B. Singh, At. Data Nucl. Data Tables **98**, 798 (2012).
[38] O. Perru *et al.*, Phys. Rev. Lett. **96**, 232501 (2006).
[39] N. Bree *et al.*, Phys. Rev. C **78**, 047301 (2008).
[40] M. Honma, T. Otsuka, B. A. Brown, and T. Mizusaki, Phys. Rev. C **69**, 034335 (2004).
[41] M. Honma, T. Otsuka, B. A. Brown, and T. Mizusaki, Euro. Phys. J. A **25**, 499 (2005).
[42] NUSHELLX@MSU, B. A. Brown, W. D. M. Rae, E. McDonald, and M. Horoi, http://people.nscl.msu.edu/~brown/resources/resources.html.

[43] R. Machleidt, Adv. Nucl. Phys. **19**, 189 (1989).
[44] A. F. Lisetskiy, B. A. Brown, M. Horoi, and H. Grawe, Phys. Rev. C **70**, 044314 (2004).
[45] B. A. Brown, A. Arima, and J. B. McGrory, Nucl. Phys. A **277**, 77 (1977).
[46] B. A. Brown, D. B. Fossan, J. M. McDonald, and K. A. Snover, Phys. Rev. C **9**, 1033 (1974).
[47] C. Vaman *et al.*, Phys. Rev. Lett. **99**, 162501 (2007).
[48] M. Horoi, B. A. Brown, T. Otsuka, M. Honma, and T. Mizusaki, Phys. Rev. C **73**, 061305(R) (2006); **74**, 059904(E) (2006).
[49] R. du Rietz *et al.*, Phys. Rev. Lett. **93**, 222501 (2004).
[50] R. Hioschen *et al.*, J. Phys. G **38**, 035104 (2011).
[51] H. L. Ma, B. G. Dong, Y. L. Yan, and X. Z. Zhang, Phys. Rev. C **80**, 014316 (2009).
[52] Y. Tsunoda, T. Otsuka, N. Shimizu, M. Honma, and Y. Utsuno, Phys. Rev. C **89**, 031301 (2014); J. Phys.: Conf. Ser. **445**, 012028 (2013).
[53] L. Coraggio, A. Covello, A. Gargano, and N. Itaco, Phys. Rev. C **89**, 024319 (2014).
[54] K. Miernik *et al.*, Phys. Rev. Lett. **111**, 132502 (2013).